JOURNAL OF MATERIALS SCIENCE 29 (1994) 4167–4176

Effect of inclusion orientation upon acoustic emission–microstructural relationships in ferritic steels

C. B. SCRUBY, H. N. G. WADLEY*
AEA Industrial Technology, Harwell Laboratory, AEA Technology, Harwell, Didcot, Oxon OXII ORA, UK

A comparison of the acoustic emission, mechanical properties and fracture behaviour of three model low-alloy steels containing manganese sulphide inclusions of varying orientation has been made as a function of tempering conditions. The majority of the inclusions existed in elliptical clusters whose major axis was aligned with the rolling direction and whose plane lay on the rolling plane. Both the yield region acoustic emission activity and ductility in the through-thickness (short transverse) sample orientation were reduced compared with the longitudinal, and to a lesser extent, transverse orientation samples. These effects are shown to be a consequence of inter-inclusion cluster shear localization in material of high yield stress and low work-hardening capacity. Because of the wide range of yield strengths and work-hardening capacities used in this study, the results extend our insight of the interactions between inclusion distribution, stress state and work-hardening capacity during ductile fracture of this class of materials.

1. Introduction

This paper is the fourth in a series in which acoustic emission has been used in conjunction with more traditional experimental techniques, to study dislocation and crack growth processes in model low-alloy ferritic steels [1–3]. Acoustic emission has been found to complement more conventional techniques such as strain and load measurement and fractography [4]. It can have extraordinarily high sensitivity, being able to detect the motion of as few as five to ten dislocations or the growth of micrometre-length microcracks provided they propagate at velocities above about a tenth the shear speed of sound (i.e. $300\,m\,s^{-1}$ in these materials) or greater. The elastic waves emitted by such defects can be passively detected with ultrasonic transducers without perturbing the process of interest. A single detector (transducer) can monitor the entire sample volume on a continuous basis. The main drawbacks of the technique are its selectivity–not all deformation and fracture events of interest are detectable–and the difficulty in identifying the precise origin of each event. However, careful experimental methods coupled with a calibrated detection system partially alleviate the second of these problems.

If the sample microstructure is systematically varied while all other variables and measurement parameters remain fixed, then changes in the emission activity can be used to identify transitions between the various types of deformation behaviour. For example, in earlier work [2] on model 3.25% Ni low-alloy steels with low sulphur content, intense acoustic emission activity was observed to occur in samples isochronally tempered in the 250–300 °C temperature range. Small-angle neutron scattering and transmission electron microscopy indicated that the emission was associated with the presence of a fine distribution of carbide precipitates. It was conjectured that these were sheared by dislocations during initial yielding, leading to local strain instabilities involving the high-speed movement of groups of dislocations that were detectable by the elastic waves radiated as acoustic emission. This interpretation was consistent with a maximum yield strength, a reduced work-hardening capacity, and a minimum non-uniform strain for the samples exhibiting the most acoustic emission.

Further work on an alloy series that was identical except for containing a higher sulphur concentration confirmed the existence of these phenomena, and provided additional insights into the generation of acoustic emission by spheroidal inclusions and the interplay between inclusions, carbides and matrix work-hardening capacity in ductile fibrous fracture [3]. Of particularly interest was the observation that the addition of spheroidal inclusions dramatically reduced the non-uniform strain of samples with low work-hardening capacity, but had a much smaller effect on samples with high work-hardening capacity. In the former case the voids nucleated at the inclusions grew little before the work-hardening capacity of the inter-inclusion ligament was exhausted and the ligament failed by shear, resulting macroscopically in a stepped or alternating shear fracture. In the latter case inclusion-

Present address: Department of Materials Science and Engineering, University of Virginia, Charlottesville, VA 22903, USA.

0022–2461

nucleated voids continued to grow until adjacent voids merged to form a single large central cavity, and macroscopically a cup and cone fracture.

These earlier studies suggested that the critical value of work-hardening capacity for transition to unstable shear depended upon the inter-inclusion spacing, which in turn is determined by the volume fraction, shape and distribution of the inclusions. The morphology of the inclusions might also be expected to have an effect upon the acoustic emission signal itself because the signal associated with decohesion should scale with the affected area resolved normal to the applied stress. For pancake-shaped inclusions, this would imply strongest emission in the short transverse orientation samples. To explore this notion further, we have prepared a set of high-sulphur samples that were extensively hot-rolled to produce elongated inclusion clusters. The samples have been tested so that the principal applied stress direction was either parallel (longitudinal orientation), or perpendicular (transverse and short transverse orientations) to the long axis of the inclusions. The results show that the effects of varying inclusion orientation on the degree of non-uniform strain are consistent with earlier observations, but the effect of orientation on the acoustic emission was not anticipated.

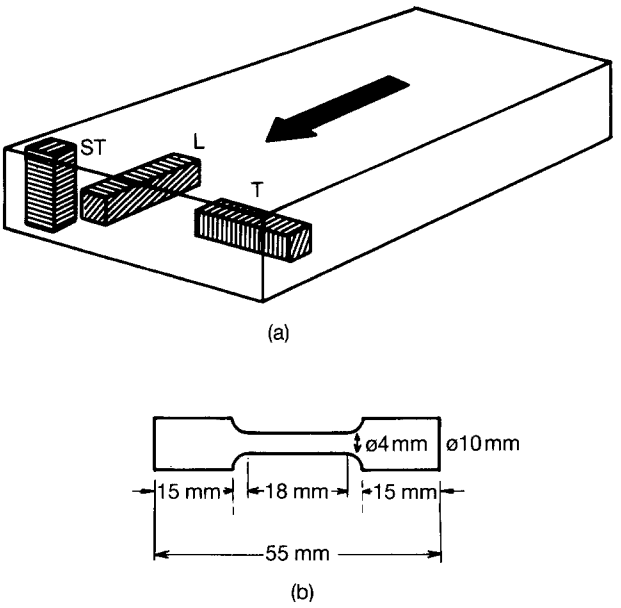

Figure 1 (a) Orientation of longitudinal (L), transverse (T) and short transverse (ST) specimens. Arrow indicates rolling direction. (b) Cylindrical tensile specimen geometry.

2. Experimental procedure

2.1. Materials

Experiments were performed on steels designated A, B and C, the same model low-alloy steels as were used for the study of spheroidal inclusion effects [3]. Their complete composition and method of casting are reported elsewhere [1–3]. They had nominally identical compositions (with the exception of carbon concentration) containing about 3.25 wt % Ni, 1.03 wt % Mn, 0.5 wt % Si and 0.07 wt % S. The carbon concentrations were 0.054, 0.197 and 0.494 wt % for steels A, B and C, respectively. With the exception of sulphur, they were similar to the low-sulphur (0.007 wt % S) steels D, E and F used previously to study cooling rate and tempering effects [1, 2].

Elongation of inclusions can be achieved by hot-rolling/forging, the degree of elongation being related to the reduction in area and temperature during hot work. Elongation can be maximized by using low finishing temperatures, when the inclusions are relatively more formable than the steel matrix. With these principles in mind, 150 mm long billets were cut from 600 mm ingots and homogenized for 2 h at 1200 °C and then allowed to cool to ~ 900 °C. They were then forged to 75 mm diameter hexagonal bar form and the finally to 25 mm thick plate at a finishing temperature of about 750 °C. The forging plane always contained the longitudinal axis of the cast ingot.

2.2. Sample preparation

It was considered important to perform tensile tests on specimens whose tensile axis was aligned with the rolling direction (L orientation), transverse to the rolling direction (T orientation) or in the short transverse direction (ST orientation) (Fig. 1). This latter orientation posed a significant problem due to the limited plate thickness in that direction. To overcome this we adopted the following procedure. First, a gauge length shorter than that of the previous studies [1–3] and a few millimetres less than the plate thickness was adopted for samples of all orientation (Fig. 1b). Then, for the ST specimen preparation, blanks were cut from the plate. Tabs of low-sulphur steel (but with the same carbon content) were attached to the ends of each blank by friction welding. This produced a very thin weld zone of excellent mechanical integrity and high ultrasonic transmission. Tensile samples were then machined from the composite blank, taking care to ensure that the weld joints were outside the gauge section so that the weld itself was not highly stressed during testing. For L and T specimen blanks of sufficient length could, of course, be machined directly from the plate, and no friction welding was necessary.

Since it was our intention to compare results with those of the earlier study [3], the samples were given a similar austenization treatment (1000 °C for 1 h, water quench) followed by an isochronal tempering heat treatment for 100 min at either 150, 240, 300, 400 or 550 °C. They were then electropolished to remove oxidation films which sometimes act as spurious acoustic emission sources.

2.3. Testing

Acoustic emission measurements were made as before [1–3] during constant strain-rate ($2.1 \times 10^{-4}\,s^{-1}$) tensile testing. Because of the shortened gauge length (20 mm instead of 40 mm previously) the crosshead displacement rate of the testing machine was halved in order to maintain a similar strain rate to the earlier work. In every other respect, procedures were the

same as before. Particular care was taken to ensure standardization of acoustic emission instrumentation so that valid comparisons could be made. This involved testing at least three samples in each condition, and using a calibration source to standardize instrumentation sensitivity prior to each test.

The principal problem for comparability with earlier work stemmed from the somewhat different gauge dimensions. Since the principal emission source was expected to be associated with deformation processes which scale with volume, we increased the gauge area from 7.07 to 12.57 mm^2 so that the gauge volume was only a few per cent less than before. However, this afforded a larger area over which subcritical fracture could develop, which would be expected to slightly enhance the emission energy from fracture.

3. Results

3.1. Microstructural characterization

Fig. 2 shows optical micrographs of the longitudinal, transverse and short transverse sections of steel B. It shows an inclusion distribution typical of all three steels. It is clear that significant inclusion elongation in the rolling direction had occurred, but that it was non-uniform. Some inclusions had aspect ratios (L:ST) as high as 10:1 while others remained almost spherical. Rolling also caused a small flattening of inclusions on the ST plane. Detailed analysis of micrographs indicated that the inclusions had an oval cross-section with approximately a 2:1 aspect ratio (i.e. T:ST).

The inclusions were not uniformly dispersed in these steels. Regions of inclusion aggregation were interspersed with regions containing only a low density of small inclusions. The low-inclusion regions were several hundred micrometres across. Earlier work [3] indicated that the majority of MnS inclusions are deposited interdendrically during solidification. The distribution of inclusions observed here is consistent with the dendrite spacing of the undeformed ingot.

Detailed studies of carbide precipitation were not made for these materials. We expect carbide distribu-

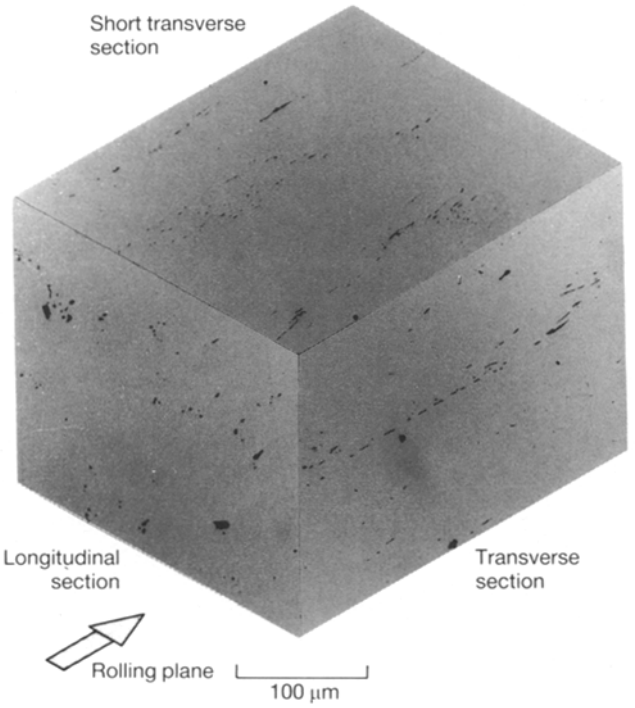

Figure 2 Optical micrographs of cross-section of longitudinal, transverse and short transverse specimens (steel B).

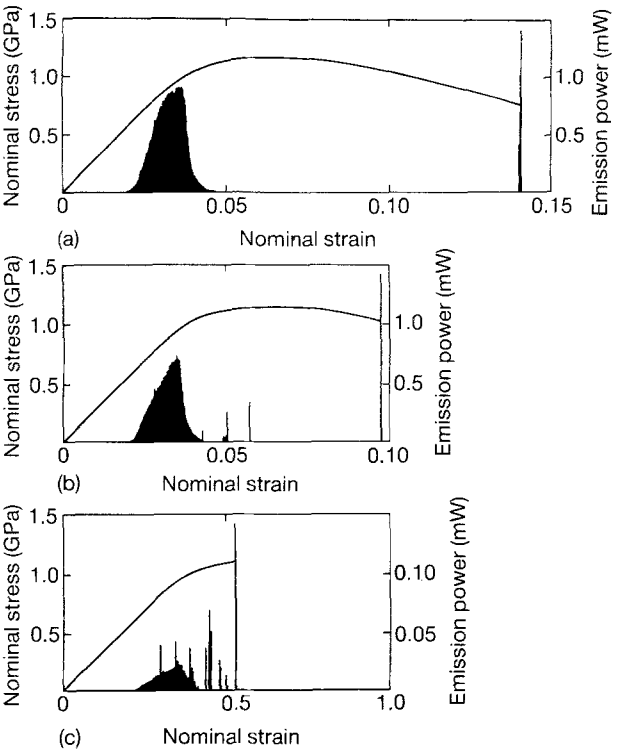

Figure 3 Effect of orientation on acoustic emission and stress as function of strain for steel B, isochronally tempered at 300 °C for 100 min: (a) L, (b) T, (c) ST orientation.

TABLE I Average of three tests for total acoustic emission from steels A, B and C

Tempering Temperature (°C)	Acoustic emission energy (mJ)								
	Steel A			Steel B			Steel C		
	L	T	ST	L	T	ST	L	T	ST
150	5.4	3.7	1.3	7.9	8.8	5.6	31.5	30.1	24.3
240	17.6	33.7	18.8	29.0	27.0	20.5	12.7	8.2	7.5
300	44.7	19.9	13.8	39.6	31.1	14.6	36.2	16.8	17.4
400	6.4	6.3	5.0	7.0	4.2	4.2	15.3	5.0	1.2
550	0.8	0.7	3.8	1.3	1.0	1.5	3.2	2.6	1.5

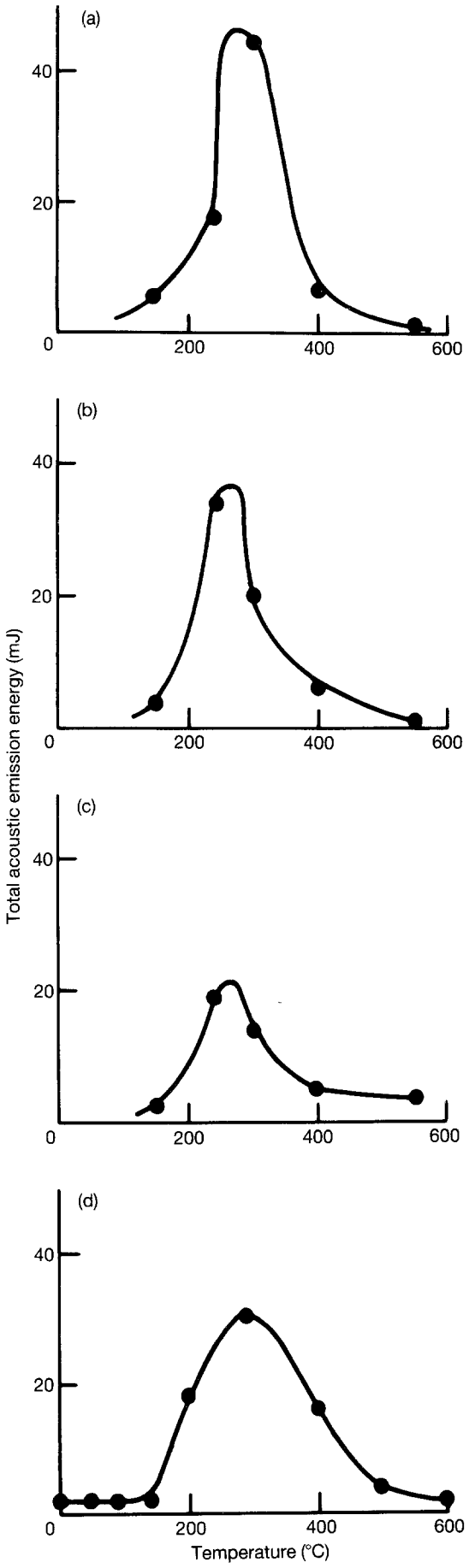

Figure 4 Effect of orientation on acoustic emission and stress as function of strain for steel A, isochronally tempered at 300 °C for 100 min: (a) L, (b) T, (c) ST, (d) spheroidal material.

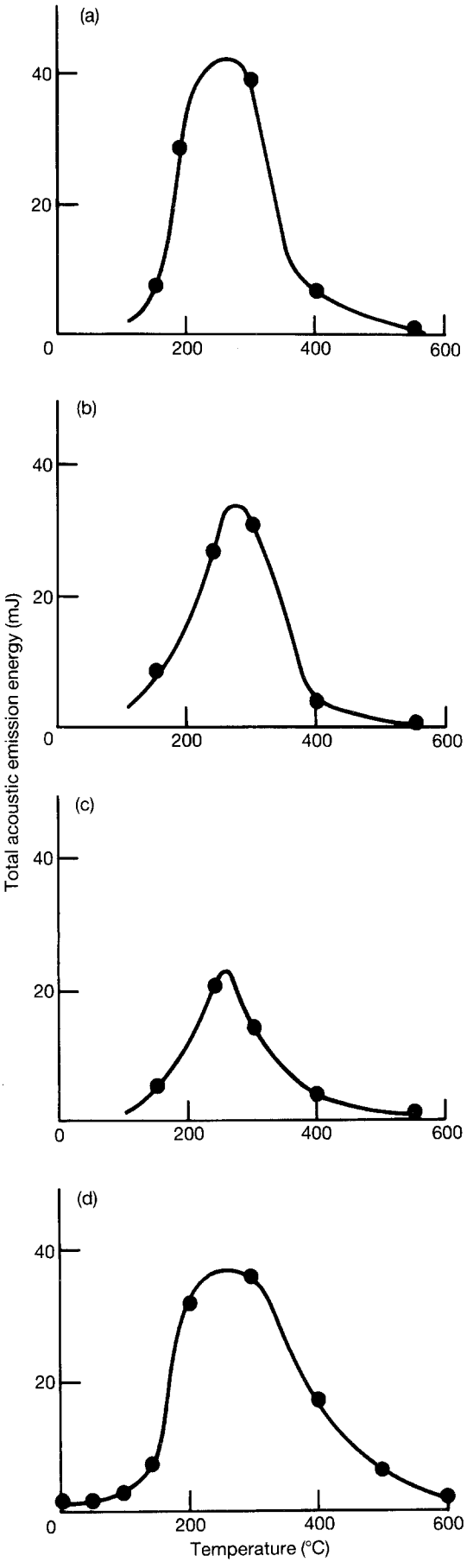

Figure 5 Emission energy as a function of isochronal tempering temperature for steel B: (a) L, (b) T, (c) ST, (d) spheroidal material.

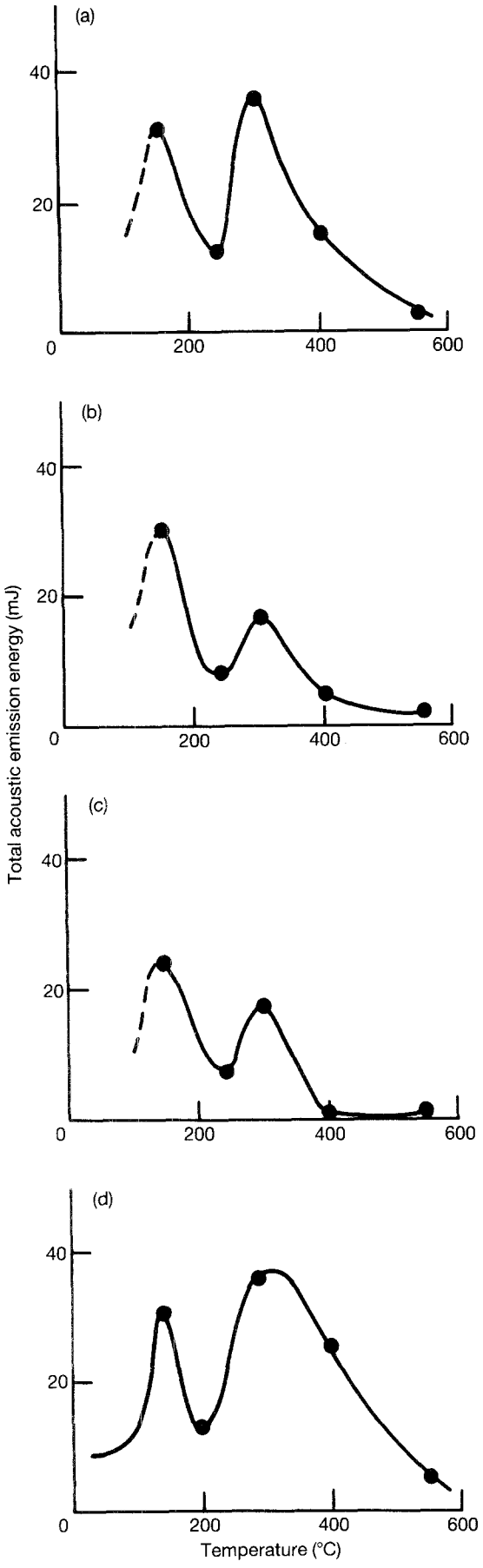

Figure 6 Emission energy as a function of isochronal tempering temperature for steel C: (a) L, (b) T, (c) ST, (d) spheroidal material.

tions to be very similar to those reported previously [2].

3.2. Acoustic emission measurements

It was observed in earlier work [2, 3] that acoustic emission activity showed a strong dependence upon isochronal tempering temperature. By testing samples of each of the three steels in the L, T and ST orientations as a function of isochronal tempering temperature, we were able systematically to evaluate the effects of inclusions morphology.

Generally, it was found that the acoustic emission–strain dependence for these materials was similar to that observed from material containing spheroidal inclusions. A fairly typical result is shown in Fig. 3 for steel B (0.197 wt %C) isochronally tempered at 300 °C for 100 min. We note that the total acoustic emission (area under curve) decreased from the L to T to ST orientation. This trend was observed for the three steels over almost the complete range of heat treatments, as can be seen in Table I. The notable exception was for steel A tempered at 550 °C, the condition with greatest work-hardening capacity.

The dependence of acoustic emission activity upon tempering temperature for each steel is shown in Figs 4 to 6. Data for spheroidal steels tested in the earlier study are also shown for comparison. Two statistically significant trends emerge from these results:

(i) The magnitude of the acoustic emission tempering peak decreases in going from the L to T to ST orientations for all but one set of samples.

(ii) Steels A and B generated a greater peak emission than steel C. This is the reverse trend to that of materials with low sulphur content [2] or containing spheroidal inclusions [3].

The earlier studies linked this tempering peak with the dislocation motion that is associated with initial yielding. These new observations suggest that the morphology and orientation of the inclusions have a profound effect on the deformation behaviour, even during the early yielding of samples.

3.3. Mechanical properties

Unlike the earlier studies, no separate mechanical property measurements were performed on a servo-hydraulic testing machine. Thus, only nominal mechanical properties could be measured from the load–extension curves recorded on the slower responding and more compliant screw-driven machine. These are tabulated in Table II.

The data indicate that the yield strength is not significantly affected by the inclusion orientation, but both the ultimate tensile strength and the plastic extension (ductility) of the ST orientation are significantly reduced. The loss of plastic extension in going from L to ST orientation was observed for all heat treatments but was particularly strong for intermediate tempering temperatures (below 400 °C). Similarly, the loss of ultimate tensile strength was also greatest for material tempered below 400 °C.

TABLE II Mechanical property parameters for high-sulphur steels of varying inclusion orientation

Orientation	Tempering Temperature (°C)	σ_y (MPa)			σ_{UTS} (MPa)			Ductility (mm)		
		A	B	C	A	B	C	A	B	C
L	150	763	991	1045	1066	1534	1085	2.49	2.24	0.01
	240	813	940	1203	1048	1352	1580	2.35	2.19	0.28
	240	716	866	1288	1010	1272	1588	2.60	1.90	0.30
	400	695	841	1043	864	1304	1270	2.68	2.42	0.40
	550	500	574	724	646	784	928	4.20	3.86	1.55
T	150	758	943	–	1068	1513	723	1.62	1.00	–
	240	799	942	–	1050	1348	1155	1.53	0.06	–
	300	753	920	577	1022	1278	620	1.59	1.17	0.01
	400	674	801	492	866	975	526	1.70	0.81	0.02
	550	500	573	340	649	771	397	3.16	2.60	0.17
ST	150	764	983	–	1008	1421	494	0.53	0.39	–
	240	788	980	–	977	1290	554	0.09	0.14	–
	300	696	833	–	980	1198	642	0.62	0.20	–
	400	689	789	–	853	987	710	0.90	0.20	–
	550	509	573	583	631	727	663	1.40	0.84	0.03

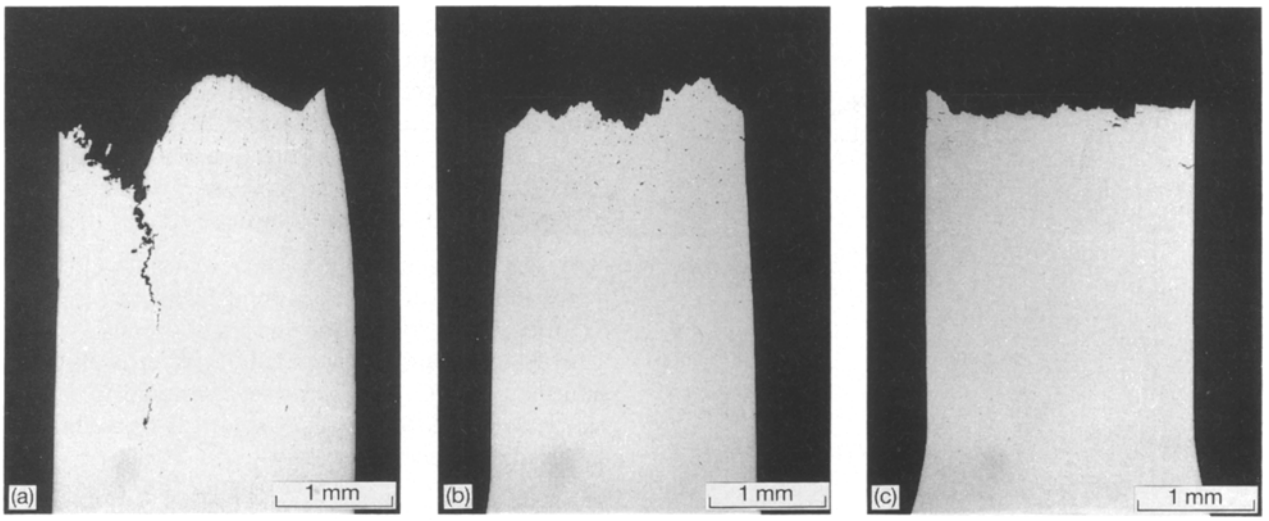

Figure 7 Optical micrographs of specimens of steel B in 300 °C tempered condition after fracture: (a) L, (b) T, (c) ST orientation.

Thus we see that the loss of acoustic emission reported above coincides with a loss of ductility and ultimate tensile strength, and hence early fracture. This important observation will be more fully discussed later.

3.4. Fractography

Both carbon content and heat treatment strongly affected the fracture in these materials. Broadly speaking, the L orientation samples tested here had a similar fracture appearance to the samples tested with spheroidal inclusions in the earlier study. The greatest effect of orientation was observed for samples of steels tempered at 300 °C (Fig. 7). The L orientation underwent a cup and cone fracture, the T orientation a stepped fracture with numerous (vertical) shear steps, while the ST orientation underwent a flat fracture with numerous horizontal subcritical microcracks near the plane of final fracture.

Fig. 8 shows higher-magnification views of the material immediately adjacent to the fracture plane. Elongated voids surround cracked inclusions in the L sample. The ST sample contained multiple horizontal microcracks formed on sheets of inclusions. The final fracture path appears to have involved shear linkage of the inclusion-nucleated void clusters. The T orientation exhibited similar microcracks, but these were of shorter horizontal length.

Scanning electron microscopy provides strong visual evidence of the role played by the inclusions in the fracture process (Fig. 9). The ST sample, though macroscopically flat, exhibited a terraced topography clearly showing that macroscopic failure occurred by the shear linkage of planes of inclusion-nucleated voids. The T orientation exhibited a zig-zag fracture path with shear occurring between rows of inclusions. Fig. 10 shows, at higher magnification, details of the fracture process. It can be seen that the depth of the inclusion-nucleated voids decreases in going from L to T to ST orientation. The effects of increasing the tempering temperature or decreasing the carbon

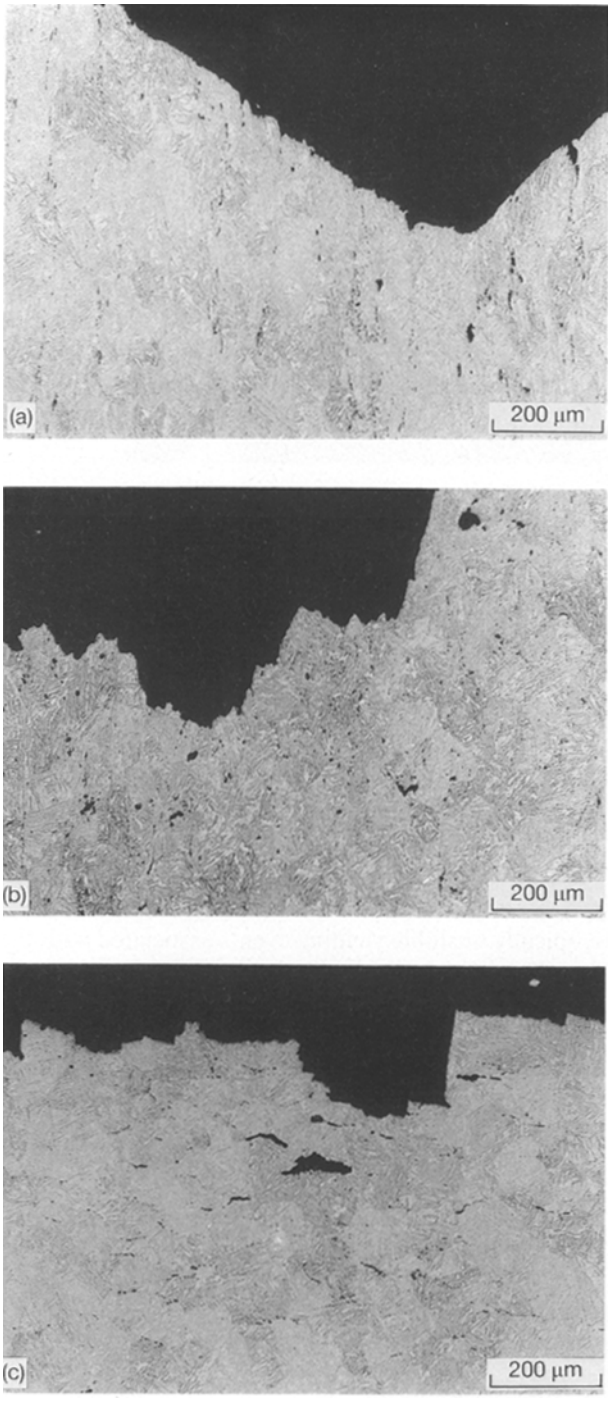

Figure 8 Optical micrographs of fracture surface of steel B in 300 °C tempered condition (2% nital etch): (a) L, (b) T, (c) ST orientation.

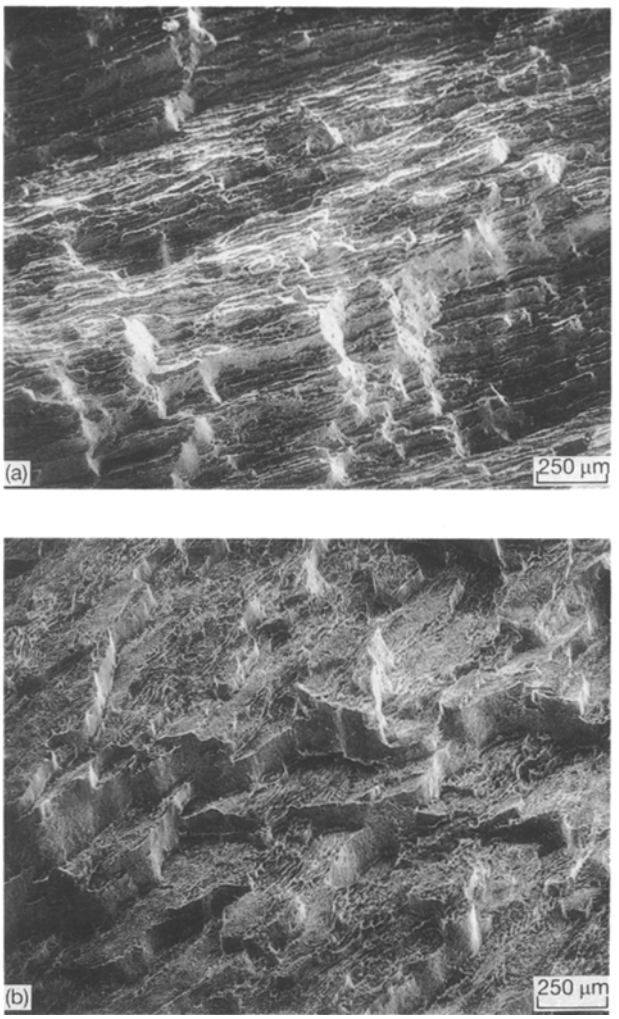

Figure 9 SEM micrographs of fracture surface of steel B in 300 °C tempered condition (2% nital etch): (a) T, (b) ST orientation.

content were to mitigate the differences in fracture behaviour, (Fig. 11).

4. Discussion

In earlier work it was shown that when spheroidal inclusions were added to steels of the same composition and heat treatment conditions as those studied here, there was a small increase in total acoustic emission for all heat treatments [2, 3]. This was consistent with the hypothesis that the inclusions were able to (a) amplify a dislocation mechanism of emission (by raising the local matrix stress) during first yielding and (b) also generate a small (additional) component of emission – perhaps due to interfacial decohesion, although this latter contribution could not be unequivocally proved.

If we sum the emission energies of all of the five tempered states tested here, we can compare the L, T and ST orientation emission activity with similarly measured and summed emission from low- and high-sulphur (spheroidal inclusion) steels reported in the earlier work [2, 3] and this is shown in Table III.

Table III reveals that the samples in the L orientation tested here generated a roughly similar amount of emission to those containing spheroidal inclusions. Their mechanical properties and fracture modes were also similar, both for each carbon concentration and as a function of isochronal tempering. Thus, we can conclude that the emission sources are similar and that elongation of the inclusions in the loading direction has a minor effect. Table III shows a reduction in emission (from that of spheroidal inclusion samples) for both the T and ST samples; in the latter case we observe the even more surprising result that the emission is reduced below the level of the low-sulphur material.

The pronounced anisotropy observed in the acoustic emission is accompanied by anisotropy in ductility

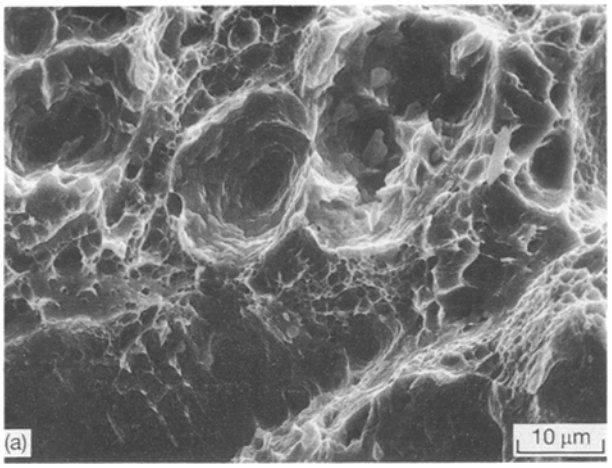

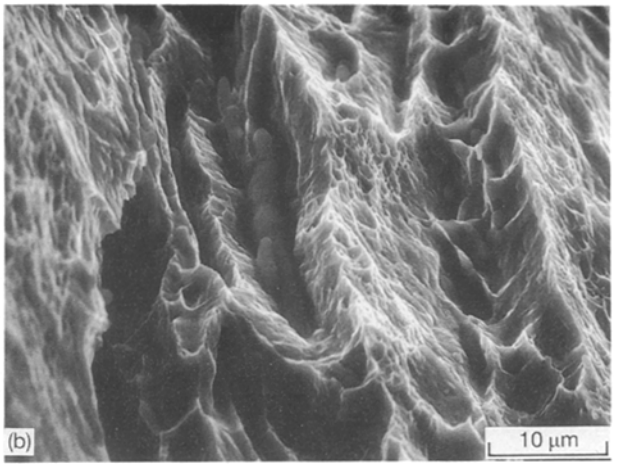

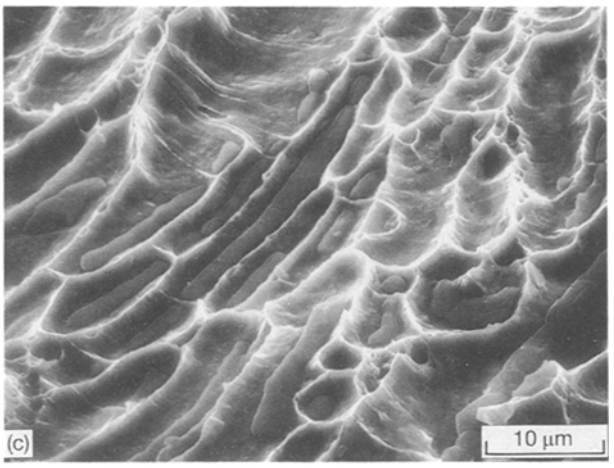

Figure 10 SEM micrographs showing effect of MnS orientation on ductile dimple morphology (steel B in 300 °C tempered condition): (a) L, (b) T, (c) ST orientation.

(as measured here by the plastic extension to fracture) and in the fracture behaviour. A smaller effect on yield and ultimate tensile strength was also noted. In general, upon changing from L to ST orientation the acoustic emission activity, ductility and strength all decreased and the fracture mode underwent a transition from a cup and cone to a more macroscopically flat fracture containing ledges and plateau (Fig 9b). These changes were most evident for material tempered at 300 °C, a condition characterized by a maximum yield strength, minimum non-uniform strain, lowest work-hardening exponent, and maximum acoustic emission associated with the dislocation mechanism of first yielding.

In earlier studies with nominally identical steels containing fewer inclusions [2], this dislocation mechanism resulted in an isochronal tempering peak in acoustic emission activity for all three steels. It was proposed that each emission originated from microscopically unstable yielding events associated with the first slip across individual lath packets of the tempered martensitic microstructure. If signals are emitted only on first yielding, and if the sources are uniformly distributed throughout the sample volume, the change in rate of emission (during straining) represents the volume rate at which the yield surface spreads through the sample, whilst the total emission is proportional to the volume of yielded material.

In earlier work on spheroidal inclusion-containing material [3], it was argued that the magnitude and range of the stress concentration around an inclusion controlled the speed of, and distance moved by, the dislocations during the microyield event, and this in turn determined the magnitude of the emission. The magnitude and range of the stress concentration in

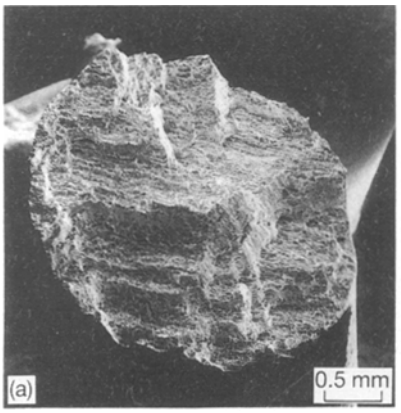

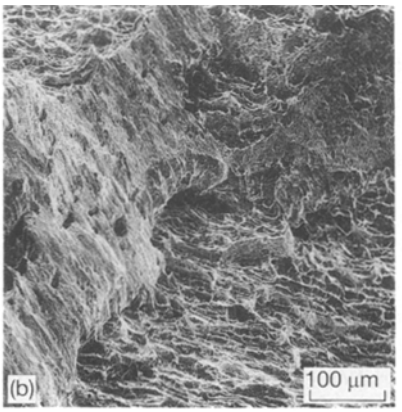

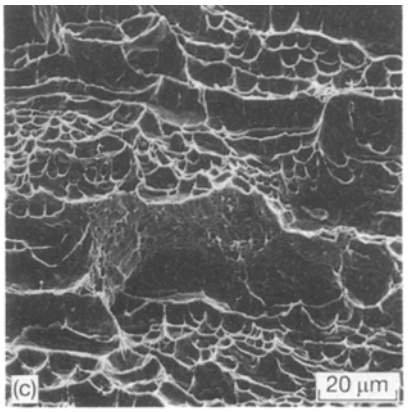

Figure 11 (a–c) SEM micrographs of steel B in the ST orientation after tempering at 550 °C.

TABLE III Comparison of acoustic emission energy for L, T and ST orientations of high-sulphur steels with that of spheroidal inclusion and low-sulphur steels

Material	Summed acoustic emission (mJ)		
	Low carbon (A, D)	Medium carbon (B, E)	High carbon (C, F)
L	74.9	84.8	98.9
T	64.3	72.1	62.7
ST	43.7	46.4	51.9
Spheroidal	67.0	93.5	110.0
Low sulphur	54.7	58.2	61.4

turn depends on the projection of the inclusion diameter on to the plane of maximum applied stress. This diameter is approximately equal for the spheroidal and longitudinal samples, consistent with their similar levels of emission activity. However, this model fails to account for the reduced emission from the T and ST orientations which both have larger projected areas on the plane of maximum stress.

An important clue to the possible reason for the emission loss lies in the fracture behaviour of these materials (see Fig. 8c). Fracture in the ST orientation occurred by shear of the ligaments linking groups of interdendritic inclusions oriented normal to the principle loading direction, as illustrated schematically in Fig. 12. These inclusions were formed during hot rolling as flat oval clusters in the rolling plane, with individual inclusions typically less than an inclusion diameter apart. For the ST orientation, the plane containing these inclusions was perpendicular to the applied load. The decohesion of isolated MnS inclusions in low-alloy steels can occur at low stresses (~ 300 MPa) [5] and from the work of Argon *et al.* [6] this can be reduced further when the stress concentrations of interacting particles overlap as they do for the ST orientation. Tracey [7] has shown that voids formed in these inclusion clusters are likely to rapidly link up (especially when the matrix hardening exponent is low) to form planar flaws (i.e. microcracks), here typically 20 μm in diameter. These flaws can be seen below the final fracture surface in Fig. 8c. Because the initiation stress for decohesion is low compared with the yield strength of the steels, it begins to occur during nominally elastic deformation.

What follows next must in general depend on the work-hardening characteristics of the deforming inter-flaw ligaments. If their work-hardening rate is high, plastic deformation processes in the ligament are accompanied by a rise in flow stress. The softening due to formation of the decohered regions is then offset by matrix hardening [6–10]. In this case it is more favourable for plasticity to spread away from the original (now work-hardened) plane of highest stress intensity. In this case the entire sample will eventually yield, followed by interinclusion necking and ultimately fracture. This is the behaviour we observe in ST material tempered at 600 °C and for all tempers of the L samples.

If, on the other hand, the matrix has a low work-hardening rate then stable plastic flow is suppressed [7] and the stress intensity on the plane of maximum

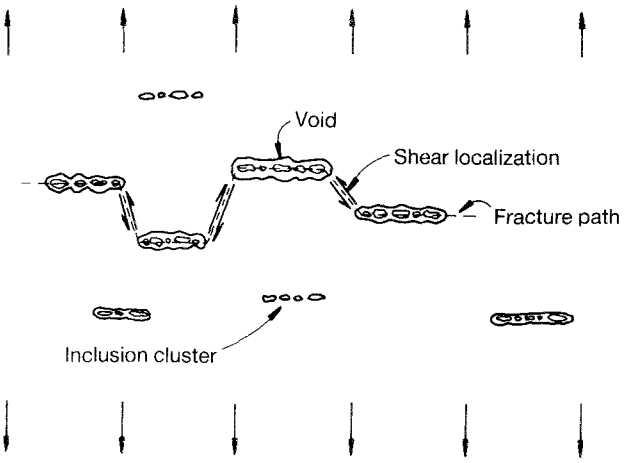

Figure 12 Shear localization fracture nucleated at inclusions in steel of ST orientation.

resolved shear stress linking the inclusions becomes sufficient to initiate a localized plastic instability [10]. If the work-hardening is very limited (as it is in samples tempered at ~ 300 °C) and the stress concentration large (i.e. the ST orientation) the instability will lead to local fracture. In the extreme case, material adjacent to the plane of maximum stress will not even reach the yield stress, so that the volume of yielded material will be smaller than for the case where the work-hardening capacity was higher. This is what we propose happened in the ST material (with severest stress concentration), the effect being most marked for the material tempered at 300 °C, which has the highest yield stress and lowest work-hardening exponent.

Thus, the loss of emission activity in going from L to ST orientation appears to be due to the reduction in the volume of sample that undergoes yielding prior to failure. The above argument predicts that ST material with a heat treatment or carbon content that results in a higher work-hardening capacity, should exhibit a smaller loss of emission. Although difficult to measure accurately, the loss of emission (compared with L and T orientations) in material tempered at 550 °C is reduced (and in steel A, with highest work-hardening, the trend is actually reversed). The fracture surfaces of these sample also exhibit more dimpling, indicative of greater plasticity (and therefore more stable flow) during interinclusion necking (Fig. 10).

The loss of emission depends upon the magnitude of the stress intensity built up around the inclusion clusters. This in turn depends on the number and size

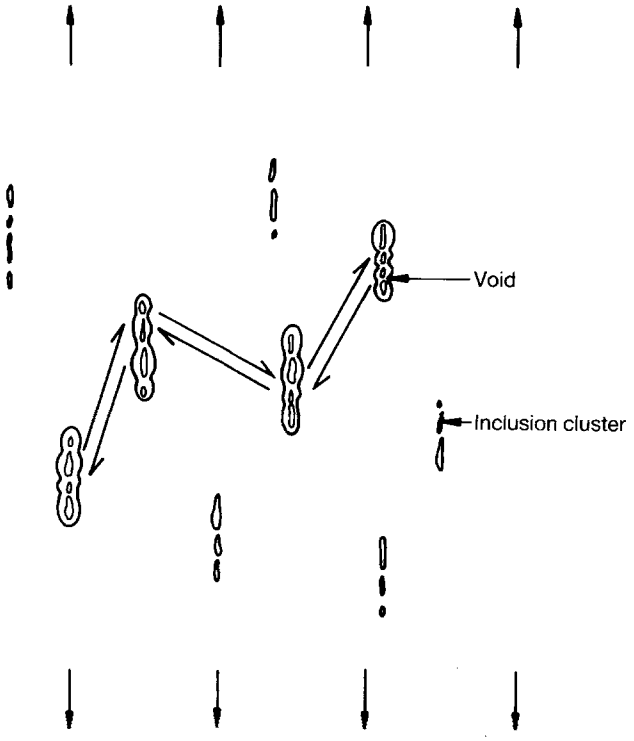

Figure 13 Ductile fracture nucleated at inclusion clusters in steel of L orientation.

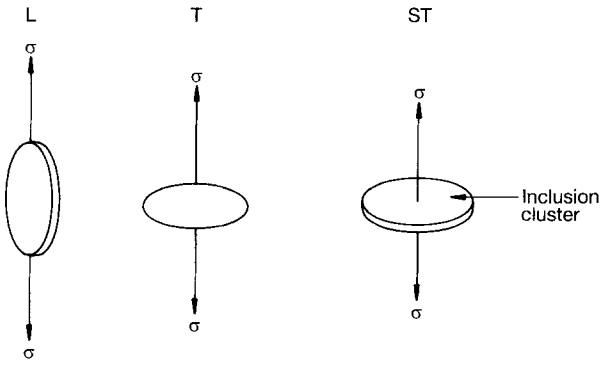

Figure 14 Orientation of oval-shaped inclusion clusters for L, T and ST specimens.

of the clusters on planes perpendicular to the applied stress axis. When the clusters are aligned along the stress axis as in the L material, the planar defects diameter in the load support direction is significantly reduced. Thus, void softening and the tendencies for strain localization are less severe. As a result, the plastic deformation is more homogeneous and void growth is promoted (Fig. 13). In the ST orientation the defects present the maximum effective diameter, and hence highest intercluster stresses. In the T orientation, the oval-shaped cluster appears as a line defect (Fig. 14) to the applied stress. This defect is intermediate in effective size to those of the L and ST orientations. Thus it is observed that there is a more limited range (than for ST material) of low work-hardening capacities which leads to shear localization.

5. Summary

Inclusion morphology and orientation with respect to the maximum stress plane have strong effects on acoustic emission, mechanical properties and fracture in hot-rolled steels containing a high volume fraction of manganese sulphide inclusions. Surprisingly, the ST samples generate reduced acoustic emission compared with L and T orientations, especially when heat-treated at $\sim 300\,^{\circ}C$ to have a low work-hardening rate. The inclusions have been shown to exist as interdendritic clusters which are ellipsoidal in shape and elongated in the rolling plane. The anisotropy in both acoustic emission and ductility for 300 °C tempered material are believed to stem from a combination of strong void softening (for ST orientation samples) coupled with a low work-hardening capacity of the matrix. This leads to unstable strain localization and fracture, in the extreme case, denying opportunity for the full sample volume to yield and generate its acoustic emission.

Acknowledgements

We gratefully acknowledge the contributions made by Drs Brian Pickering and John Hudson during discussions of this work, P. Lane for help in conducting experiments and Dr Uri Admon for assistance with some of the fractography. We also wish to acknowledge funding of the research by the Ministry of Defence (PE) through ARE (Holton Heath).

References

1. H. N. G. WADLEY and C. B. SCRUBY, *J. Mater. Sci.* **26** (1991) 5777.
2. C. B. SCRUBY and H. N. G. WADLEY, *ibid.* **28** (1993) 2501.
3. H. N. G. WADLEY and C. B. SCRUBY, *ibid.* **28** (1993) 2517.
4. H. N. G. WADLEY, in "Acoustic Emission: A Quantitative NDE Technique for the Study of Fracture," Proceedings of ONR Symposium on Solid Mechanics Research for QNDE, North Western University, 1985.
5. H. N. G. WADLEY, D. C. FURZE, C. B. SCRUBY and B. L. EYRE, *Metal Sci.* **13** (August 1979) 451.
6. A. S. ARGON, J. IM and R. SAFOGLU, *Met. Trans.* **6A** (1975) 825.
7. D. M. TRACEY, *Eng. Fract. Mech.* **3** (1971) 301.
8. M. SAJE, J. PAN and A. NEEDLEMAN, *Int. J. Fract.* **19** (1982) 163.
9. A. NEEDLEMAN and J. R. RICE, in " Mechanisms of Sheet Metal Forming", edited by D. P. Koistinen and N-M Wang, (Plenum, New York, 1978) p. 237.
10. J. W. HUTCHINSON and T. TVERGAARD, in "Fracture Mechanics: Perspectives and Directions (Twentieth Symposium)", ASTM STP 1020, edited by R. P. Wei and R. P. Gangloff (American Society for Testing and Materials, Philadelphia, 1989) p. 61.

Received 14 September
and accepted 8 October 1993